

A First-Order Systems Least-Squares Finite Element Method for the Poisson-Boltzmann Equation

Stephen D. Bond^{a,1}, Jehanzeb Hameed Chaudhry^{a,*,2}, Eric C. Cyr^{b,2}, Luke N. Olson^{a,3}

^aDepartment of Computer Science, University of Illinois, Urbana, IL 61801

^bSandia National Laboratory, Albuquerque, NM, 87185

Abstract

The Poisson-Boltzmann equation is an important tool in modeling solvent in biomolecular systems. In this paper, we focus on numerical approximations to the electrostatic potential expressed in the regularized linear Poisson-Boltzmann equation. We expose the flux directly through a first-order system form of the equation. Using this formulation, we propose a system that yields a tractable least-squares finite element formulation and establish theory to support this approach. The least-squares finite element approximation naturally provides an *a posteriori* error estimator and we present numerical evidence in support of the method. The computational results highlight optimality in the case of adaptive mesh refinement for a variety of molecular configurations. In particular, we show promising performance for the Born ion, Fasciculin 1, methanol, and a dipole, which highlights robustness of our approach.

Key words: Poisson-Boltzmann, implicit solvent, finite elements, least-squares, adaptive refinement

PACS: 82.20.Wt, 83.10.Rs, 87.10.Kn, 87.10.Ed

2000 MSC: 65N30, 92C40

1. Introduction

Solvent plays a critical role in determining the structure and function of biomolecular systems. However, the explicit representation of solvent at a molecular level is often intractable due to the range of scales required. Moreover, properly modeling solvent interactions with molecules is computationally expensive due to the complexity of the atomistic interactions that must be sampled over multiple configurations. As such, implicit solvent models, such as the Poisson-Boltzmann model [1] and Generalized Born model [2], confront this difficulty by treating the solvent as a bulk continuum.

The focus of this work is on numerical solutions to the Poisson-Boltzmann equation (PBE), which approximates the mean solvent forces by assuming the ions are distributed according to the Boltzmann distribution. This results in a unique electrostatic potential described by this implicit solvent model [3]. In particular, we seek a numerical solution of the linearization of the regularized PBE (RPBE). The use of a regularized formulation [3], is required because the original statement of the PBE yields singularities in the electrostatic potential. Regularization overcomes this issue by analytically subtracting the singularities from the electrostatic potential yielding a modified version of the original PDE. To further simplify the problem, and focus on the efficacy of our discretization, we linearize the RPBE. The linearized version has many of the same challenges as the RPBE, however it features reduced computation cost [4] while remaining a physically accurate perturbation to the fully nonlinear problem [5].

A number of different directions for numerically solving the Poisson-Boltzmann equation have been pursued. Approaches such as finite difference and finite volume methods [6–15], finite elements methods [3, 16–22], boundary element methods [23–34], and integral equations [35, 36] have been developed for this problem. Yet, as the complexity of applications increases so do the demands on the numerical approximation, and we are motivated to investigate additional computational tools that provide a medium for more robust and efficient simulation.

*Corresponding author

Email addresses: `sdbond@illinois.edu` (Stephen D. Bond), `jhameed2@illinois.edu` (Jehanzeb Hameed Chaudhry), `eccyr@sandia.gov` (Eric C. Cyr), `lukeo@illinois.edu` (Luke N. Olson)

¹Supported in part by NSF-CCF 08-30578

²Supported in part by University of Illinois CSE Fellowship

³Supported in part by NSF-DMS 07-46676

In this paper, we focus on a variational setting for the PBE due to the underlying theoretical support for numerical methods and the established analysis of the equation. In particular, we propose a least-squares finite element formulation of the linear regularized Poisson-Boltzmann equation. Least-squares finite element methods offer a viable approach to efficient and accurate approximation. The least-squares method we follow begins by reforming the partial differential equation as a first-order system. A functional is then constructed based on the residual equations of the first-order system, and is minimized. A first-order system least-squares (FOSLS) approach to finite elements has shown to be effective for numerous problems. In particular, elliptic problems [37, 38] with discontinuous coefficients [39–41] are theoretically competitive and numerically plausible.

The existing FOSLS theory motivates our treatment of the PBE, yet the theoretical properties for the FOSLS form we pose in Section 3 are not fully developed. We establish these results and confirm the existence of a unique solution for our problem. We propose a first-order system for the PBE in Section 3 that correctly addresses the jump discontinuity inherent in the problem. The PBE is described through a dielectric coefficient, $\epsilon(x)$, and Debye-Hückel parameter, $\bar{\kappa}(x)$, that are discontinuous across an interface. Proper treatment of the flux term across this interface is critical to the variational formulation. To this end, we propose a unique form of the flux that both captures the underlying physics and yields a system amenable to a least-squares minimization.

The goal of this paper is to outline a least-squares finite element method for use with existing computational tools, such as the Finite Element Toolkit (FETk) [42], which uses piecewise linear elements over tetrahedral tessellations of single domains. The result is a competitive and straightforward finite element method for the PBE using adaptive mesh refinement. Adaptive refinement using finite elements has been studied for the Poisson-Boltzmann equation in a Galerkin formulation [18, 19]. These approaches focus on resolution of the singularities in the original PDE. Here, we use the functional provided by the least-squares formulation to guide refinement with similar success. Treatment of the interface condition is automatic in our formulation of the problem, naturally capturing the physics around the interface while still being amenable to approximation by standard finite elements.

The remainder of the paper is organized as follows. In Section 2, we summarize the PBE, its regularization and linearization, and the general problem domain. We outline the FOSLS terminology in Section 3 and introduce our formulation of the method. Moreover, we establish theoretically the use our formulation and discuss implications and techniques for computational simulation. In Section 4, we provide numerical evidence of effectiveness of the FOSLS approach for a number of molecular systems. The method is shown to be effective for problems with known solutions (Born ion), for more complicated structures (Fasciculin 1 and methanol), and for a problem with low regularity (dipoles).

2. Poisson Boltzmann Equation

The Poisson-Boltzmann equation models the electrostatic activity between molecules in an ionic solvent. In this model, it is assumed that the ions in the solvent are distributed according to the Boltzmann distribution and that the potential of the mean force on a particle is simply the charge of the ion times the electrostatic potential. This yields the general Poisson-Boltzmann equation [5],

$$-\nabla \cdot (\epsilon(x) \nabla \phi(x)) = 4\pi \rho_f(x) + 4\pi \sum_{j=1}^{n_s} c_j^s Q_j^s \lambda_j(x) \exp \left[\frac{-1}{k_B T} Q_j^s \phi(x) \right], \quad (1a)$$

$$\lim_{\|x\| \rightarrow \infty} \phi(x) = 0. \quad (1b)$$

Here, ϕ is the unknown electrostatic potential, ϵ is the dielectric coefficient, ρ_f is the fixed charge distribution in the solute (biomolecule), k_B is the Boltzmann constant, and T is the temperature. It is assumed that the solvent is composed of n_s species of ions, each with charge Q_j^s and concentration c_j^s . The accessibility of the j th ion-species to a point, x , in space is described by $\lambda_j(x)$.

For a solute in a 1:1 electrolyte solvent (e.g. NaCl), the charge of each ion species is ± 1 unit charge, and the general Poisson-Boltzmann equation simplifies [1] to

$$-\nabla \cdot (\epsilon(x) \nabla \phi(x)) + \bar{\kappa}^2(x) \left(\frac{k_B T}{e_c} \right) \sinh \left(\frac{e_c \phi(x)}{k_B T} \right) = 4\pi \sum_{i=1}^m Q_i \delta(x - x_i), \quad (2a)$$

$$\lim_{\|x\| \rightarrow \infty} \phi(x) = 0. \quad (2b)$$

Here, we have further assumed that solute contains a total of m fixed point charges, with the i th charge, Q_i , centered at position x_i . The resulting distribution, ρ_f , is a linear combination of Dirac delta functions, $\delta(x - x_i)$.

The domain for the problem, \mathbb{R}^3 , is subdivided into a molecular region, Ω_m , a solvent region, Ω_s^∞ , and an interface between the two, denoted by Γ . The solute is surrounded by solvent, which is represented as a continuum over the subdomain $\Omega_s^\infty = \mathbb{R}^3 \setminus \overline{\Omega_m}$. In some Poisson-Boltzmann models, an additional ion exclusion or Stern layer is present between Ω_s and Ω_m . The Stern layer provides separation between the solute and the ions of the solvent. As a result, the dielectric matches the dielectric in the solvent region and the ionic strength is zero ($\bar{\kappa} = 0$). In this paper we focus on the more challenging issue of the jump in the dielectric, and neglect the Stern layer. The subdomains for a typical biomolecular solute are shown in Figure 1. The dielectric coefficient, $\epsilon(x)$, and modified

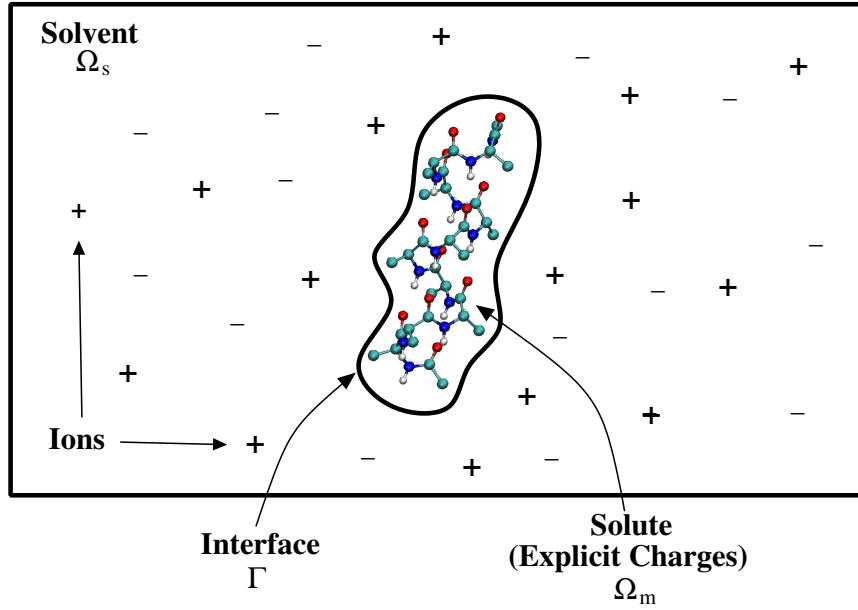


Figure 1: Subdomains for the Poisson-Boltzmann equation

Debye-Hückel parameter, $\bar{\kappa}(x)$, describe the accessibility of the solvent to the solute and are defined on $\Omega_m \cup \Omega_s^\infty$ by the piecewise constant functions

$$\epsilon(x) = \begin{cases} \epsilon_m & x \in \Omega_m \\ \epsilon_s & x \in \Omega_s^\infty \end{cases} \quad \text{and} \quad \bar{\kappa}^2(x) = \begin{cases} 0 & x \in \Omega_m \\ \bar{\kappa}_s^2 = \epsilon_s \frac{8\pi N_A e_c^2}{1000 k_B T} I_s & x \in \Omega_s^\infty \end{cases}. \quad (3)$$

Here, ϵ_m and ϵ_s are positive constants, N_A is Avogadro's number, and e_c is the charge of a proton. The ionic strength, I_s , is a physical parameter which varies depending on the solvent.

For computational reasons, the unbounded solvent domain, Ω_s^∞ , is typically truncated at a finite radius from the “center” of the molecule, which gives rise to a bounded solvent domain, Ω_s . Dirichlet boundary conditions are imposed to capture the asymptotic behavior of the solution on an unbounded domain. Combining this with the change of variables, $\tilde{u}(x) = e_c \phi(x)/k_B T$, results in a dimensionless Poisson-Boltzmann equation on the spherical domain $\Omega = \Omega_m \cup \Omega_s \cup \Gamma$:

$$-\nabla \cdot (\epsilon(x) \nabla \tilde{u}(x)) + \bar{\kappa}^2(x) \sinh \tilde{u}(x) = \frac{4\pi e_c}{k_B T} \sum_{i=1}^m Q_i \delta(x - x_i), \quad x \in \Omega_m \cup \Omega_s, \quad (4a)$$

$$\tilde{u}(x) = g(x), \quad x \in \partial\Omega_s, \quad (4b)$$

$$\left\| \epsilon(x) \frac{\partial \tilde{u}(x)}{\partial \mathbf{n}} \right\|_\Gamma = 0, \quad x \in \Gamma. \quad (4c)$$

where the jump at the interface is defined as

$$\left\| \epsilon(x) \frac{\partial \tilde{u}(x)}{\partial \mathbf{n}} \right\|_\Gamma = \lim_{\alpha \rightarrow 0^+} \epsilon(x + \alpha \mathbf{n}) \frac{\partial \tilde{u}(x + \alpha \mathbf{n})}{\partial \mathbf{n}} - \epsilon(x - \alpha \mathbf{n}) \frac{\partial \tilde{u}(x - \alpha \mathbf{n})}{\partial \mathbf{n}},$$

with \mathbf{n} as the unit normal to the interface Γ .

The boundary conditions are prescribed using a linear combination of Helmholtz Green's functions,

$$g = \frac{e_c}{k_B T} \sum_{i=1}^m \frac{Q_i}{\epsilon_s |x - x_i|} \exp\left(\frac{-\bar{\kappa}_s |x - x_i|}{\sqrt{\epsilon_s}}\right). \quad (5)$$

In contrast to (2a), the principal equation is defined over each subdomain and an interface condition is introduced on Γ . This restatement makes explicit the normal continuity implied by the strong form divergence of $\epsilon(x)\nabla\phi$ across the interface Γ in the original PBE.

We denote the standard Sobolev spaces as $L^2(\Omega)$ and $H^k(\Omega)$, for $k \geq 0$. $H^k(\Omega)$ consists of functions over Ω having square integrable (weak) derivatives of order up to k . The norms on $L^2(\Omega)$ and $H^k(\Omega)$ are expressed as $\|\cdot\|_{0,\Omega}$ and $\|\cdot\|_{k,\Omega}$, with the $L^2(\Omega)$ inner product written $(\cdot, \cdot)_{0,\Omega}$. In addition, we define the Hilbert spaces

$$\begin{aligned} H(\text{div}; \Omega) &:= \{\mathbf{q} \in L^2(\Omega)^3 : \nabla \cdot \mathbf{q} \in L^2(\Omega)\}, \\ H_0(\text{div}; \Omega) &:= \{\mathbf{q} \in H(\text{div}; \Omega) : \mathbf{n} \cdot \mathbf{q} = 0 \text{ on } \partial\Omega\}, \\ H_0^1(\Omega) &:= \{u \in H^1(\Omega) : u = 0 \text{ on } \partial\Omega\}, \end{aligned}$$

with norms

$$\|\mathbf{q}\|_{\text{div},\Omega}^2 = \|\mathbf{q}\|_{0,\Omega}^2 + \|\nabla \cdot \mathbf{q}\|_{0,\Omega}^2, \quad (6)$$

$$\|u\|_{1,\Omega}^2 = \|u\|_{0,\Omega}^2 + \|\nabla u\|_{0,\Omega}^2. \quad (7)$$

One difficulty with (2a) is regularity. The right-hand side $4\pi \sum_i Q_i \delta(x - x_i)$ is not in $H^{-1}(\Omega)$, i.e., the dual space of $H_0^1(\Omega)$. Practically, the right-hand side induces singularities in \tilde{u} at the solute atom centers x_i . These singularities are the familiar consequence of solute-solute electrostatic interactions satisfying Coulomb's law. However, finite element and finite difference methods often require more smoothness in order to guarantee convergence. Following [3], we overcome this issue by decomposing \tilde{u} into

$$\tilde{u} = u + u_c, \quad (8)$$

where u is an unknown smooth function and u_c is a known singular function. The Coulomb function, u_c , satisfies the Poisson equation

$$-\epsilon_m \nabla \cdot \nabla u_c(x) = \frac{4\pi e_c}{k_B T} \sum_{i=1}^m Q_i \delta(x - x_i), \quad (9)$$

and absorbs the singularities in \tilde{u} . Combining (8) with (4), we obtain the regularized PBE or RPBE

$$\begin{aligned} -\nabla \cdot \epsilon(x) \nabla u(x) + \bar{\kappa}^2(x) \sinh(u(x) + u_c(x)) &= \nabla \cdot (\epsilon(x) - \epsilon_m) \nabla u_c(x), & x \in \Omega_s \cup \Omega_m, \\ u(x) &= g(x) - u_c(x), & x \in \partial\Omega, \\ \left\| \epsilon(x) \frac{\partial u(x)}{\partial \mathbf{n}} \right\|_{\Gamma} &= (\epsilon_m - \epsilon_s) \frac{\partial u_c(x)}{\partial \mathbf{n}}, & x \in \Gamma. \end{aligned} \quad (10)$$

Since $\bar{\kappa}(x)$ and $\epsilon(x) - \epsilon_m$ are zero inside Ω_m , we avoid evaluating the Coulomb potential, u_c , near the singularities present at each point charge, $x_i \in \Omega_m$. This yields a right-hand side in (10) that is a well-defined distribution in $H^{-1}(\Omega)$ and, as a result, equation (10) is a well-defined nonlinear second-order elliptic equation with a unique weak solution u in $H^1(\Omega)$ [3].

A simplified version of (10) is the linear regularized Poisson-Boltzmann equation, which is obtained by linearizing the hyperbolic sine:

$$-\nabla \cdot \epsilon(x) \nabla u(x) + \bar{\kappa}^2(x) u(x) = \nabla \cdot (\epsilon(x) - \epsilon_m) \nabla u_c(x) - \bar{\kappa}^2(x) u_c(x), \quad x \in \Omega_s \cup \Omega_m, \quad (11a)$$

$$u(x) = g(x) - u_c(x), \quad x \in \partial\Omega, \quad (11b)$$

$$\left\| \epsilon(x) \frac{\partial u(x)}{\partial \mathbf{n}} \right\|_{\Gamma} = (\epsilon_m - \epsilon_s) \frac{\partial u_c(x)}{\partial \mathbf{n}}, \quad x \in \Gamma. \quad (11c)$$

Physically, the linearization reduces the ionic response of the solvent to the solute. This approximation is acceptable unless the solute is highly charged [4]. In this case the magnitude of the electrostatic potential is large, and the approximation $\sinh(u) \approx u$ is not accurate [1].

3. FOSLS Formulation of PBE

The First-Order System Least Squares (FOSLS) finite element method is an alternative to standard and mixed Galerkin finite element methods [43]. FOSLS begins by converting the PDE to a first order system. Using the new set of equations, a functional is then defined whose minimizer solves the original PDE.

FOSLS offers a number of potential advantages over traditional methods. The functional is minimized using a variational principle, giving rise to a symmetric bilinear form. A discretization based on this form leads to a symmetric positive-definite linear system, which is ideal for solvers such as preconditioned conjugate gradient. Also, the bilinear form is often elliptic with respect to a practical norm, and as a result the finite element spaces do not need to satisfy the discrete inf-sup condition of Ladyzhenskaya-Babuška-Brezzi [44], unlike mixed methods. A practical consequence is that basic finite element spaces, e.g. continuous piecewise linear polynomials, may be used for all variables.

The FOSLS functional also provides a local *a posteriori* error estimate. Such estimates are complicated for other methods, but the FOSLS residual norm provides a straightforward and accurate estimate for our problem. This local error estimate is used for adaptively refining a mesh in our numerical experiments and we highlight the effectiveness of this tool.

Least-Squares finite element methods are not without limitation, however. The introduction of new variables to formulate the first-order system ultimately increases the degrees of freedom and complexity in computing the solution. This is not necessarily a disadvantage as the new variables are often physically meaningful and are often needed elsewhere in the simulation. For example, the FOSLS formulation of the PBE introduces a secondary “flux” variable, which is used to effectively compute potential of the mean force required in the solution of the Steady-State Smoluchowski Equation [45]. Another potential drawback is that FOSLS requires more regularity than might be present in the problem to ensure optimal error estimates. Optimal error estimates using a Least-Squares approach for PBE can be derived through a multi-domain approach for such problems [46]. In this paper, we also use adaptive refinement to overcome these issues of computational complexity, yielding optimal convergence rates in our numerical experiments.

A typical approach to forming a first-order system of (11) over a single domain Ω is to introduce a flux, $\tilde{\mathbf{q}} = \epsilon(x)\nabla u$ (e.g., see [39]). The resulting first-order system is

$$\tilde{\mathbf{q}} - \epsilon\nabla u = 0 \quad \text{in } \Omega, \quad (12a)$$

$$-\nabla \cdot \tilde{\mathbf{q}} + \bar{\kappa}^2 u = \nabla \cdot (\epsilon(x) - \epsilon_m)\nabla u_c - \bar{\kappa}^2 u_c \quad \text{in } \Omega, \quad (12b)$$

$$u = g - u_c \quad \text{on } \partial\Omega. \quad (12c)$$

An application of Green’s theorem on this system shows that across any surface in Ω with normal \mathbf{n} , $\mathbf{n} \cdot \tilde{\mathbf{q}}$ is continuous. In particular, solution to system (12) satisfies,

$$\left[\left[\tilde{\mathbf{q}} \cdot \mathbf{n} \right] \right]_{\Gamma} = 0 \quad x \in \Gamma.$$

However, since $\tilde{\mathbf{q}} = \epsilon\nabla u$, equation (11c) implies,

$$\left[\left[\tilde{\mathbf{q}} \cdot \mathbf{n} \right] \right]_{\Gamma} = (\epsilon_m - \epsilon_s)\nabla u_c(x) \cdot \mathbf{n} \quad x \in \Gamma.$$

This implies $\tilde{\mathbf{q}} \cdot \mathbf{n}$ is not continuous across the interface Γ , and hence, a least squares approach based on system (12) is an incorrect formulation for solving the RPBE.

For a well-posed FOSLS formulation to system (11), we need to define a first-order variable \mathbf{q} , whose normal component is not only continuous across the interface, but also satisfies the interface condition required by RPBE. To ensure these conditions, we define $\mathbf{q} = \epsilon(x)\nabla u + (\epsilon(x) - \epsilon_m)\nabla u_c$, which results in,

$$\mathbf{q}/\epsilon(x) - \nabla u = ((\epsilon(x) - \epsilon_m)/\epsilon(x))\nabla u_c \quad \text{in } \Omega, \quad (13a)$$

$$-\nabla \cdot \mathbf{q} + \bar{\kappa}^2 u = -\bar{\kappa}^2 u_c \quad \text{in } \Omega, \quad (13b)$$

$$u = g - u_c \quad \text{on } \partial\Omega, \quad (13c)$$

$$\mathbf{n} \times \mathbf{q} = \mathbf{n} \times (\epsilon_s \nabla g + (\epsilon(x) - \epsilon_m)\nabla u_c) \quad \text{on } \partial\Omega. \quad (13d)$$

Now equations (11c) and (13) imply,

$$\left[\left[\mathbf{q} \cdot \mathbf{n} \right] \right]_{\Gamma} = 0 \quad x \in \Gamma.$$

We now pose our problem in abstract form and establish a unique solution. To simplify the analysis we consider homogeneous Dirichlet boundary conditions. Using a standard lifting argument, we obtain

$$\begin{aligned} \mathbf{q}/\epsilon(x) - \nabla u &= ((\epsilon(x) - \epsilon_m)/\epsilon(x))\nabla u_c & \text{in } \Omega, \\ -\nabla \cdot \mathbf{q} + \bar{\kappa}^2 u &= -\bar{\kappa}^2 u_c, & \text{in } \Omega, \\ u &= 0 & \text{on } \partial\Omega, \\ \mathbf{n} \times \mathbf{q} &= 0 & \text{on } \partial\Omega. \end{aligned} \quad (14)$$

The least-squares functional based on (13) is as follows. For $\mathbf{q} \in H_0(\text{div}; \Omega)$ and $u \in H_0^1(\Omega)$, we define

$$G(\mathbf{q}, u; u_c) = \|\mathbf{q}/\epsilon(x) - \nabla u - ((\epsilon(x) - \epsilon_m)/\epsilon(x))\nabla u_c\|_{0,\Omega}^2 + \|-\nabla \cdot \mathbf{q} + \bar{\kappa}^2 u + \bar{\kappa}^2 u_c\|_{0,\Omega}^2. \quad (15)$$

The solution of (13) solves the minimization problem

$$G(\mathbf{q}, u; u_c) = \min_{(\mathbf{r}, v) \in H_0(\text{div}; \Omega) \times H_0^1(\Omega)} G(\mathbf{r}, v; u_c) \quad (16)$$

and leads to the variational problem

$$\mathcal{F}(\mathbf{q}, u; \mathbf{r}, v) = \ell(\mathbf{r}, v), \quad (17)$$

where the bilinear form \mathcal{F} and linear functional ℓ are

$$\mathcal{F}(\mathbf{q}, u; \mathbf{r}, v) = (\mathbf{q}/\epsilon - \nabla u, \mathbf{r}/\epsilon - \nabla v)_{0,\Omega} + (-\nabla \cdot \mathbf{q} + \bar{\kappa}^2 u, -\nabla \cdot \mathbf{r} + \bar{\kappa}^2 v)_{0,\Omega}, \quad (18)$$

$$\ell(\mathbf{r}, v) = -(\bar{\kappa}^2 u_c, -\nabla \cdot \mathbf{r} + \bar{\kappa}^2 v)_{0,\Omega} + (((\epsilon - \epsilon_m)/\epsilon)\nabla u_c, \mathbf{r}/\epsilon - \nabla v)_{0,\Omega}. \quad (19)$$

3.1. Ellipticity of FOSLS functional

To show the variational problem (17) is well-posed, it is sufficient to prove that $G(\mathbf{q}, u; 0)^{\frac{1}{2}}$ defines a norm equivalent to the $H(\text{div}) \times H^1$ norm (Theorem 1). This result also ensures that our finite element solution is the best approximation to the true solution under the norm defined by $G(\mathbf{q}, u; 0)$. Before proving this norm equivalence, we start by stating and proving a lemma, which will be used in the proof of Theorem 1.

Lemma 1. *Let $h(x)$ and $k(x)$ be two positive bounded functions on Ω , i.e. $0 < c_1 < h(x) < c_2$ and $0 < c_1 < k(x) < c_2$ for all $x \in \Omega$, where c_1 and c_2 are constants. Then there exists positive constants α_1 and α_2 such that*

$$\alpha_1 \hat{\mathcal{F}}(\mathbf{q}, u; \mathbf{q}, u) \leq \mathcal{F}(\mathbf{q}, u; \mathbf{q}, u) \leq \alpha_2 \hat{\mathcal{F}}(\mathbf{q}, u; \mathbf{q}, u), \quad (20)$$

where the bilinear form $\hat{\mathcal{F}}$ is defined as

$$\hat{\mathcal{F}}(\mathbf{q}, u; \mathbf{r}, v) = (\sqrt{h}(\mathbf{q}/\epsilon - \nabla u), \sqrt{h}(\mathbf{r}/\epsilon - \nabla v))_{0,\Omega} + (\sqrt{k}(-\nabla \cdot \mathbf{q} + \bar{\kappa}^2 u), \sqrt{k}(-\nabla \cdot \mathbf{r} + \bar{\kappa}^2 v))_{0,\Omega}. \quad (21)$$

Proof of Lemma 1. Taking $\alpha_1 = c_2^{-1}$ and $\alpha_2 = c_1^{-1}$ gives the desired result. \square

Theorem 1. *The bilinear form \mathcal{F} defines a norm equivalent to the $H(\text{div}) \times H^1$ norm. That is, there exists positive constants γ_1 and γ_2 such that*

$$\mathcal{F}(\mathbf{q}, u; \mathbf{r}, v) \leq \gamma_1 (\|\mathbf{q}\|_{H(\text{div})}^2 + \|u\|_{1,\Omega}^2)^{1/2} (\|\mathbf{r}\|_{H(\text{div})}^2 + \|v\|_{1,\Omega}^2)^{1/2} \quad (22)$$

and

$$\mathcal{F}(\mathbf{q}, u; \mathbf{q}, u) \geq \gamma_2 (\|\mathbf{q}\|_{H(\text{div})}^2 + \|u\|_{1,\Omega}^2). \quad (23)$$

Proof. A proof for the general case is given in [37]. Here we offer a proof for our specific case, to obtain sharper constants of ellipticity; our proof is in the same spirit as a proof presented in [39].

First we prove boundedness of \mathcal{F} (equation (22)). An application of Cauchy-Bunyakovsky-Schwarz inequality to (18) leads to

$$\mathcal{F}(\mathbf{q}, u; \mathbf{r}, v) \leq (\mathcal{F}(\mathbf{q}, u; \mathbf{q}, u))^{1/2} (\mathcal{F}(\mathbf{r}, v; \mathbf{r}, v))^{1/2}. \quad (24)$$

Using the fact that ϵ is bounded away from zero in Ω yields

$$\begin{aligned} \mathcal{F}(\mathbf{q}, u; \mathbf{q}, u) &= \|\mathbf{q}/\epsilon - \nabla u\|_{0,\Omega}^2 + \|-\nabla \cdot \mathbf{q} + \bar{\kappa}^2 u\|_{0,\Omega}^2 \\ &\leq \gamma_3 (\|\mathbf{q}\|_{0,\Omega}^2 + \|\nabla u\|_{0,\Omega}^2 + \|\nabla \cdot \mathbf{q}\|_{0,\Omega}^2 + \|u\|_{0,\Omega}^2) \\ &= \gamma_3 (\|\mathbf{q}\|_{H(\text{div})}^2 + \|u\|_{1,\Omega}^2), \end{aligned} \quad (25)$$

where $\gamma_3 = \max(2, 2\bar{\kappa}^4, 2\epsilon^{-2}) = \max(2, 2\bar{\kappa}_s^4, 2\epsilon_m^{-2}, 2\epsilon_s^{-2})$. Combining equations (25) and (24) proves boundedness of \mathcal{F} .

To prove coercivity, we consider a modified bilinear form, as defined by (21). We define $h(x)$ and $k(x)$ as:

$$h(x) = \begin{cases} \epsilon(x) & x \in \Omega_m \\ \tau\epsilon(x) & x \in \Omega_s \end{cases} \quad \text{and} \quad k(x) = \begin{cases} 1 & x \in \Omega_m \\ \tau/\bar{\kappa}_s^2 & x \in \Omega_s, \end{cases} \quad (26)$$

where τ is a constant such that $0 < \tau < 1$.

We can decompose the integral over Ω and evaluate \mathcal{F} over Ω_s and Ω_m ,

$$\hat{\mathcal{F}}(\mathbf{q}, u; \mathbf{q}, u) = \hat{\mathcal{F}}(\mathbf{q}, u; \mathbf{q}, u)|_{\Omega_s} + \hat{\mathcal{F}}(\mathbf{q}, u; \mathbf{q}, u)|_{\Omega_m} \quad (27)$$

where

$$\hat{\mathcal{F}}(\mathbf{q}, u; \mathbf{q}, u)|_{\Omega_s} = \|\sqrt{\tau}\mathbf{q}/\sqrt{\epsilon} - \sqrt{\tau}\sqrt{\epsilon}\nabla u\|_{0,\Omega_s}^2 + \|\sqrt{\tau}/\bar{\kappa}_s \nabla \cdot \mathbf{q} + \sqrt{\tau}\bar{\kappa}_s u\|_{0,\Omega_s}^2 \quad (28)$$

and

$$\hat{\mathcal{F}}(\mathbf{q}, u; \mathbf{q}, u)|_{\Omega_m} = \|\mathbf{q}/\sqrt{\epsilon} - \sqrt{\epsilon}\nabla u\|_{0,\Omega_m}^2 + \|\nabla \cdot \mathbf{q}\|_{0,\Omega_m}^2. \quad (29)$$

Integration by parts shows that

$$\int_{\Omega_m} \nabla \cdot \mathbf{q} u + \int_{\Omega_m} \mathbf{q} \cdot \nabla u - \int_{\Gamma} u \mathbf{q} \cdot \mathbf{n}_m = 0, \quad (30)$$

where \mathbf{n}_m is the unit normal at Γ , pointing from the solute region into the solvent region. Applying this result to (29), we obtain

$$\begin{aligned} \hat{\mathcal{F}}(\mathbf{q}, u; \mathbf{q}, u)|_{\Omega_m} &= \|\mathbf{q}/\sqrt{\epsilon}\|_{0,\Omega_m}^2 + \|\sqrt{\epsilon}\nabla u\|_{0,\Omega_m}^2 - 2 \int_{\Omega_m} \mathbf{q} \cdot \nabla u + \|\nabla \cdot \mathbf{q}\|_{0,\Omega_m}^2 + 2\tau \int_{\Omega_m} \nabla \cdot \mathbf{q} u \\ &\quad + 2\tau \int_{\Omega_m} \mathbf{q} \cdot \nabla u - 2\tau \int_{\Gamma} u \mathbf{q} \cdot \mathbf{n}_m + \tau^2 \|\mathbf{q}\|_{0,\Omega_m}^2 - \tau^2 \|u\|_{0,\Omega_m}^2 \\ &= \|\mathbf{q}/\sqrt{\epsilon} + (\tau - 1)\sqrt{\epsilon}\nabla u\|_{0,\Omega_m}^2 + \|\nabla \cdot \mathbf{q} + \tau u\|_{0,\Omega_m}^2 - \tau^2 \|u\|_{0,\Omega_m}^2 \\ &\quad + (2\tau - \tau^2) \|\sqrt{\epsilon}\nabla u\|_{0,\Omega_m}^2 - 2\tau \int_{\Gamma} u \mathbf{q} \cdot \mathbf{n}_m. \end{aligned} \quad (31)$$

Similarly, using integration by parts on equation (28) yields

$$\begin{aligned} \hat{\mathcal{F}}(\mathbf{q}, u; \mathbf{q}, u)|_{\Omega_s} &= \|\sqrt{\tau}\mathbf{q}/\sqrt{\epsilon}\|_{0,\Omega_s}^2 + \|\sqrt{\tau}\sqrt{\epsilon}\nabla u\|_{0,\Omega_s}^2 \\ &\quad - 2\tau \int_{\Omega_s} \mathbf{q} \cdot \nabla u + \|\sqrt{\tau}\nabla \cdot \mathbf{q}/\bar{\kappa}_s\|_{0,\Omega_s}^2 + \|\sqrt{\tau}\bar{\kappa}_s u\|_{0,\Omega_s}^2 - 2\tau \int_{\Omega_s} \nabla \cdot \mathbf{q} u \\ &= \|\sqrt{(\tau/\bar{\kappa}_s)}\nabla \cdot \mathbf{q}\|_{0,\Omega_s}^2 + \|\sqrt{\tau}\mathbf{q}/\sqrt{\epsilon}\|_{0,\Omega_s}^2 + \|\sqrt{\tau}\sqrt{\epsilon}\nabla u\|_{0,\Omega_s}^2 + \|\sqrt{\tau}\bar{\kappa}_s u\|_{0,\Omega_s}^2 - 2\tau \int_{\Gamma} u \mathbf{q} \cdot \mathbf{n}_s, \end{aligned} \quad (32)$$

where $\mathbf{n}_s = -\mathbf{n}_m$ is the unit normal along Γ , pointing from the solvent domain into the solute.

Using the Poincaré-Friedrichs inequality, we can assume

$$\|u\|_{0,\Omega}^2 \leq \lambda \|\nabla u\|_{0,\Omega}^2, \quad \text{with } \lambda > 1. \quad (33)$$

From equations (27), (31), (32), (33) and choosing $\tau = \frac{1}{2\lambda} < 1$ we have

$$\begin{aligned} \hat{\mathcal{F}}(\mathbf{q}, u; \mathbf{q}, u) &= \|\sqrt{\tau}\mathbf{q}/\sqrt{\epsilon}\|_{0,\Omega_s}^2 + \|\sqrt{\tau}\sqrt{\epsilon}\nabla u\|_{0,\Omega_s}^2 + \|\sqrt{\tau}\nabla \cdot \mathbf{q}/\bar{\kappa}_s\|_{0,\Omega_s}^2 + \|\sqrt{\tau}\bar{\kappa}_s u\|_{0,\Omega_s}^2 \\ &\quad + \|\mathbf{q}/\sqrt{\epsilon} + (\tau - 1)\sqrt{\epsilon}\nabla u\|_{0,\Omega_m}^2 + \|\nabla \cdot \mathbf{q} + \tau u\|_{0,\Omega_m}^2 - \tau^2 \|u\|_{0,\Omega_m}^2 + (2\tau - \tau^2) \|\sqrt{\epsilon}\nabla u\|_{0,\Omega_m}^2 \\ &\geq \|\sqrt{\tau}\sqrt{\epsilon}\nabla u\|_{0,\Omega_s}^2 + (2\tau - \tau^2) \|\sqrt{\epsilon}\nabla u\|_{0,\Omega_m}^2 - \tau^2 \|u\|_{0,\Omega_m}^2 \\ &\geq \tau \|\sqrt{\epsilon}\nabla u\|_{0,\Omega}^2 - \tau^2 \|u\|_{0,\Omega}^2 \geq (\tau - \lambda\tau^2) \|\sqrt{\epsilon}\nabla u\|_{0,\Omega}^2 \\ &= \frac{1}{4\lambda} \|\sqrt{\epsilon}\nabla u\|_{0,\Omega}^2 \geq \alpha_3 \|\nabla u\|_{0,\Omega}^2, \end{aligned} \quad (34)$$

where $\alpha_3 = \frac{1}{4\lambda} \min(\epsilon_m, \epsilon_s)$.

Now from equation (20), we get

$$\mathcal{F}(\mathbf{q}, u; \mathbf{q}, u) \geq \alpha_4 \|\nabla u\|_{0,\Omega}^2, \quad (35)$$

where $\alpha_4 = \alpha_1 \alpha_3$. From the Poincaré-Friedrichs inequality (33), we find

$$\mathcal{F}(\mathbf{q}, u; \mathbf{q}, u) \geq \alpha_5 \|u\|_{0,\Omega}^2. \quad (36)$$

Moreover,

$$\|\mathbf{q}/\epsilon\|_{0,\Omega}^2 \leq 2(\|\mathbf{q}/\epsilon - \nabla u\|_{0,\Omega}^2 + \|\nabla u\|_{0,\Omega}^2) \leq 2\left(1 + \frac{1}{\alpha_4}\right) \mathcal{F}(\mathbf{q}, u; \mathbf{q}, u),$$

and hence $\mathcal{F}(\mathbf{q}, u; \mathbf{q}, u) \geq \alpha_6 \|\mathbf{q}\|_{0,\Omega}^2$ for $\alpha_6 = \alpha_4 [2(1 + \alpha_4) \max(\epsilon_s, \epsilon_m)]^{-1}$. Similarly,

$$\|\nabla \cdot \mathbf{q}\|_{0,\Omega}^2 \leq 2(\|\nabla \cdot \mathbf{q} - \bar{\kappa}^2 u\|_{0,\Omega}^2 + \|\bar{\kappa}^2 u\|_{0,\Omega}^2) \leq 2(1 + \bar{\kappa}_s^4 \alpha_5) \mathcal{F}(\mathbf{q}, u; \mathbf{q}, u), \quad (37)$$

and thus $\mathcal{F}(\mathbf{q}, u; \mathbf{q}, u) \geq \alpha_7 \|\nabla \cdot \mathbf{q}\|_{0,\Omega}^2$ for $\alpha_7 = [2(1 + \bar{\kappa}_s^4 \alpha_5)]^{-1}$.

Taking $\gamma_2 = \min(\alpha_4, \alpha_5, \alpha_6, \alpha_7)$ completes the proof. \square

The FOSLS functional (15) is $H(\text{div}) \times H^1$ equivalent. In some FOSLS formulations, a curl term of the form $\nabla \times (\mathbf{q}/\epsilon) = 0$ is added to problem formulation (e.g., [39]), yielding a $H^1 \times H(\text{div}) \cap H(\text{curl})$ equivalent FOSLS functional. The extra constraint is motivated by $\tilde{\mathbf{q}} = \epsilon \nabla u$, which implies $\nabla \times \tilde{\mathbf{q}}/\epsilon = 0$ (c.f., [47], Theorem 2.9). However, for our case, we cannot take the curl of \mathbf{q}/ϵ . This follows from our definition of $\mathbf{q} = \epsilon \nabla u + (\epsilon - \epsilon_m) \nabla u_c$; the curl of \mathbf{q}/ϵ is undefined at the interface. Hence we do not add the curl term to the formulation.

Traditionally, developing an effective error estimator for use in local adaptive refinement is challenging. Error estimators based on the Galerkin method are not immediately obvious from the problem formulation and local error bounds for the PBE can be complicated to derive [3]. In contrast, the FOSLS framework directly provides a natural error indicator through the functional. The local value of FOSLS functional is an *a posteriori* lower error bound, and, under some restrictions on mesh refinement, the bound can be shown to be a sharp theoretical error estimate [48]. We exploit this fact and build an adaptive refinement scheme based on the value of the FOSLS functional.

Let $G_\tau(\mathbf{q}, u; u_c)$ be the value of the FOSLS functional (15) restricted to element τ . Note that if S is the set of elements comprising the mesh, then

$$G(\mathbf{q}, u; u_c) = \sum_{\tau \in S} G_\tau(\mathbf{q}, u; u_c).$$

Let $\mu_\tau = \sqrt{G_\tau(\mathbf{q}, u; u_c)}$ and $\mu_{\max} = \max_{\tau \in S} \mu_\tau$. We mark simplex τ for refinement if $\mu_\tau \geq \gamma \mu_{\max}$ where $\gamma \in (0, 1)$.

Our strategy is relatively straightforward, yet more advanced marking strategies based on the ‘‘solvation free-energy’’ [49] and FOSLS [48, 50] functionals have been proposed in the literature. However, in our numerical experiments, we did not find a significant difference in performance when the marking strategy is varied for our problem. When compared on the same mesh, FOSLS requires more memory and CPU time than the standard second-order Galerkin method. However, the meshes produced by the corresponding adaptive refinement schemes are different, and the FOSLS approach is often able to achieve a more accurate solution with less refinement. As a result, the FOSLS approach is often more efficient than a standard second-order Galerkin method. The effectiveness of our scheme is highlighted in Section 4.

4. Numerical Experiments

We use a tetrahedral mesh of Ω with globally continuous piecewise linear finite functions (P1 elements) and implement our finite element method and mesh refinement in FETK [42]. The meshes are generated using the Geometry-preserving Adaptive Mesher (GAMer), which is designed to produce simplicial meshes of molecular volumes and interfaces [51]. As a result, the solvent domain has a spherical outer boundary and the mesh is conforming at the interface of the solvent and molecule regions. For the first four numerical experiments, we choose $\epsilon_m = 1$, $\epsilon_s = 78$, and $\bar{\kappa}_s = 0.918168$, which corresponds to a typical ionic strength of 0.1M. In these experiments, we solve for the regularized potential and strongly impose boundary conditions. The experiments are performed on the Born ion, Fasciculin 1, methanol, and a simple dipole. Let \mathbf{q}^h and u^h be our finite-element solution, and \mathbf{q} and u the true solution. We verify convergence to the solution by monitoring the square-root of FOSLS functional, $G(\mathbf{q}^h, u^h; u_c)^{\frac{1}{2}}$, since the FOSLS functional measures the error in the norm induced by G : $G(\mathbf{q}^h, u^h; u_c)^{\frac{1}{2}} = G(\mathbf{q}^h - \mathbf{q}, u^h - u; 0)^{\frac{1}{2}}$. Therefore convergence of the FOSLS functional to zero implies convergence of our finite element solution to the true solution. We use uniform octal refinement and adaptive refinement to test the effectiveness of your method, with adaptive refinement being carried out by longest edge bisection. Since $G(\cdot, \cdot, 0)^{\frac{1}{2}}$ is equivalent to $H(\text{div}) \times H^1$ norm, a standard finite-element error estimate implies optimal convergence rate to be $O(h)$ using uniform refinement with piecewise linear basis functions [37]. This optimal estimate assumes the problem to be H^2 regular. The convergence rate degrades as the solution becomes less smooth. We examine this scenario (dipole), and show that we still recover optimal convergence using adaptive refinement. In the following results, we refer to $G(\mathbf{q}^h, u^h; u_c)^{\frac{1}{2}}$ as the FOSLS norm and plot convergence rates normalized by the largest value.

Finally, to validate the solutions generated by our implementation, we compute the solvation free energy of transcription factor PML (PDB code 1BOR). We compare the computed value with values found in the literature.

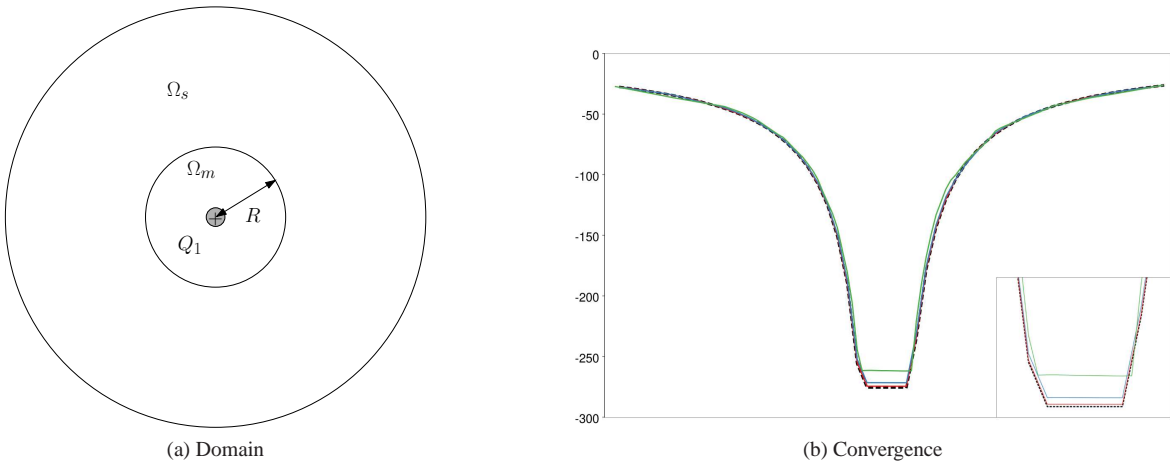


Figure 2: Born Ion

Born Ion

Due to the complex geometries associated with molecules there are few analytical solutions to the PBE or linearized PBE; however, it is possible to find an expression for the potential of a spherical ion in a solvent [52]. This system is referred to as the Born ion after its author Max Born [53]. The domain consists of a spherical solute of radius R with a single point charge Q_1 at its center. The solute is surrounded by an unbounded solvent, Ω_s , as depicted in Figure 2a.

Writing the linear regularized PBE in spherical coordinates yields

$$\begin{aligned} -\frac{1}{r^2} \frac{d}{dr} \left(\epsilon(r) r^2 \frac{d}{dr} u(r) \right) + \bar{\kappa}^2(r) u(r) &= -\bar{\kappa}^2(r) u_c(r), & r \neq R, \\ \left[\epsilon(r) \frac{d}{dr} u(r) \right]_{\Gamma} &= (\epsilon_m - \epsilon_s) \frac{d}{dr} u_c(r), & r = R \\ u(\infty) &= 0 \end{aligned}$$

where $\omega = \bar{\kappa}_s / \sqrt{\epsilon_s}$. Following [52], we obtain the analytic solution

$$u(r) = \begin{cases} C_1 \exp[-\omega(r - R)] / r - C_2 / r, & R \leq r, \\ (C_1 - C_2) / R, & 0 \leq r < R, \end{cases}$$

where

$$C_1 = \frac{e_c Q_1}{k_B T} \frac{1}{(1 + \omega R) \epsilon_s}, \quad \text{and} \quad C_2 = \frac{e_c Q_1}{k_B T} \frac{1}{\epsilon_m}.$$

Figure 3a displays the convergence of the reaction potential u in the L^2 norm, where the normalized L^2 error is plotted as a function of N , the number of points in the mesh. In three-dimensions, we observe a convergence rate of nearly $O(h^2)$ for uniform refinement, which corresponds to $O(N^{-2/3})$. On the other hand, for adaptive refinement, we observe a slightly better convergence rate. Figure 3b displays the FOSLS functional residual as the mesh is refined. In three-dimensions, a convergence rate of $O(h)$ corresponds to $O(N^{-1/3})$. We see that the FOSLS functional decreases nearly linear in h . During refinement, we ensure that new points on the solute/solvent interface lie on the analytically determined spherical boundary of the interface. As an example of convergence, in Figure 2b we display a slice of the true solution, a numerical solution on the initial mesh, and numerical solutions after two successive steps of uniform mesh refinement.

Fasciculin 1

The Born ion is a useful test case as the analytical solution is known; however, it is not a realistic simulation. To study the effectiveness of the FOSLS formulation on a realistic protein, we compute the regularized potential of Fasciculin 1 (1FAS in the Protein Data Bank) in an implicit solvent. 1FAS is a neurotoxin found in green mamba venom [54]. The dynamics and electrostatics of the Fasciculin 2 variant of this protein in its role as an acetylcholinesterase inhibitor have been studied in [55] and [56], where the electrostatics are argued to be

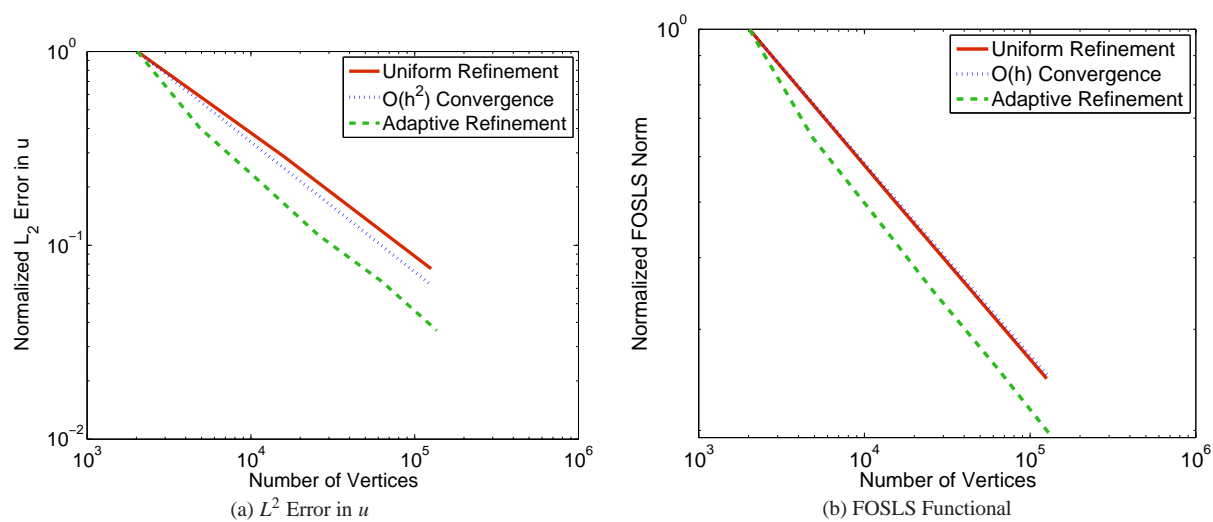


Figure 3: Convergence Rates of Born Ion

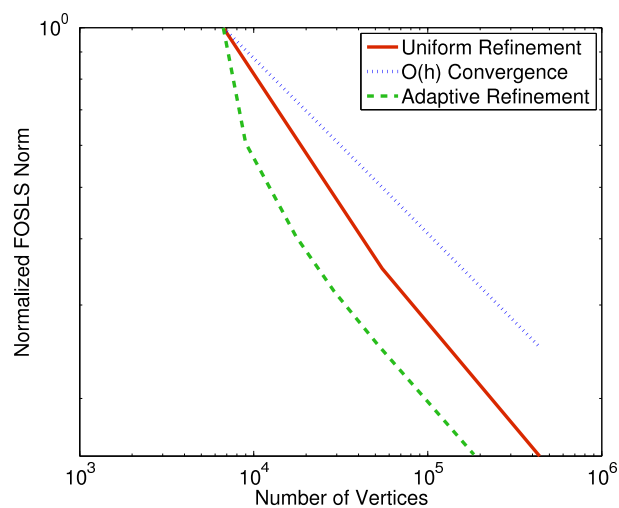


Figure 4: Fasciculin 1

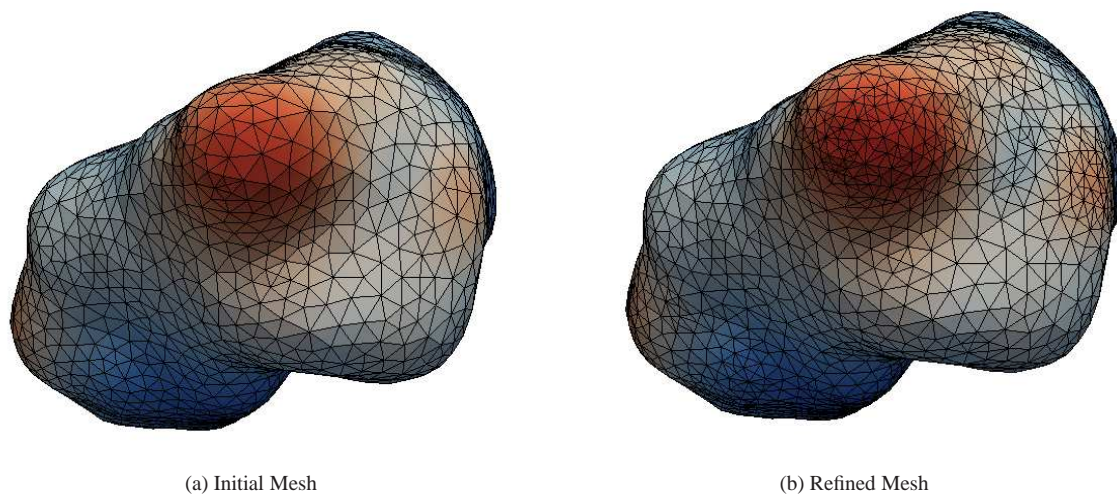
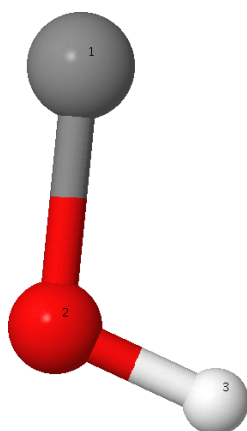


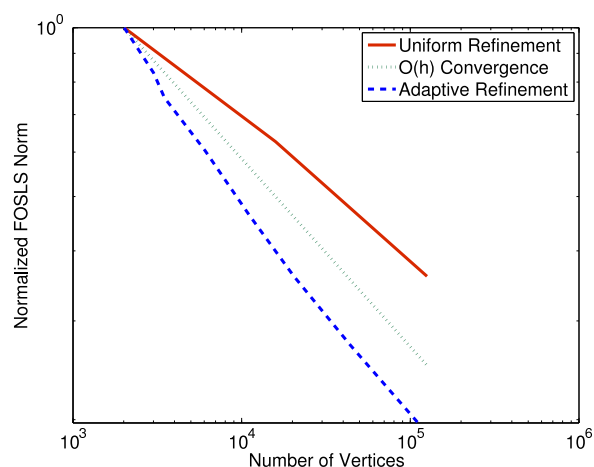
Figure 5: Adaptive refinement around the solute/solvent interface of Fasciculin 1

important to its function. In our experiments we use the description of the molecule specified in the PDB file from the Protein Data Bank and strip off water molecules using VMD [57]. The molecule region is not perfectly spherical, and we do not expect the solution to be symmetric as we did in the case of Born ion. It is assumed that the initial mesh defines the solute and solvent regions so that the solute/solvent interface in this case is polygonal and defined by the initial mesh. Consequently, refinement adds points to the polygonal interface. While the analytical solution for Fasciculin 1 is not known, we are able to monitor the convergence of FOSLS functional.

Figure 4 shows the normalized convergence rate of FOSLS functional. Both uniform and adaptive refinement perform well: the convergence rate is better than $O(h)$ for both cases. Figure 5 depicts adaptive refinement around the Fasciculin molecule. The adaptive scheme refines aggressively around the areas where the solution is changing sharply.

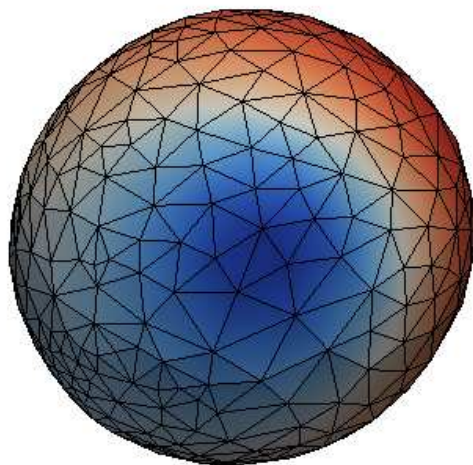


(a) Molecular Model

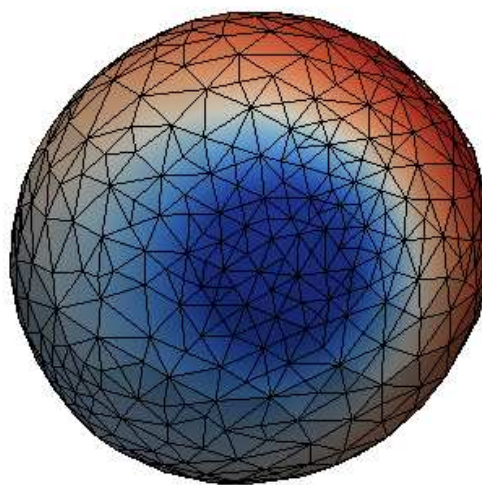


(b) Convergence

Figure 6: Methanol



(a) Initial Mesh



(b) Refined Mesh

Figure 7: Adaptive refinement around the solute/solvent interface of methanol

Methanol

We examine our method in the more challenging setting of a methanol molecule, obtained from the APBS software package [11]. The model consists of three charged spheres representing charge groups: CH_3 and H with positive charges of 0.27 and 0.43 respectively, and an O atom with a negative charge of 0.7. The net charge on the molecule is zero. Figure 6a displays the methanol molecule.

We assume again that the initial mesh properly defines the solute and solvent regions. Figure 6b displays the FOSLS functional as a function of the number of vertices in the mesh. We see from the plot that the FOSLS functional does decrease, but the convergence is slightly less than $O(h)$. On the other hand, adaptive refinement is ideal for this problem since the solution varies sharply across the interface, indicating areas where local refinement is useful. As Figure 6b shows, adaptive refinement yields slightly better than $O(h)$ convergence. The performance of adaptive refinement is shown in Figures 7 and 8, where the regularized electrostatic potential around the interface is displayed. Figure 7 shows the initial mesh and an adaptively refined mesh. Figure 8 displays a slice of the regularized solution, which highlights the areas in which the solution changes rapidly and also that the solution is not symmetric.

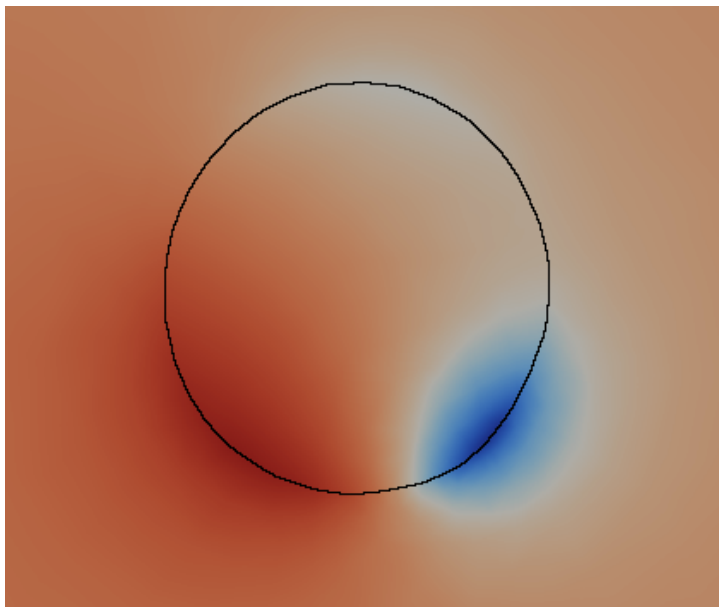


Figure 8: Methanol: Solution around the interface

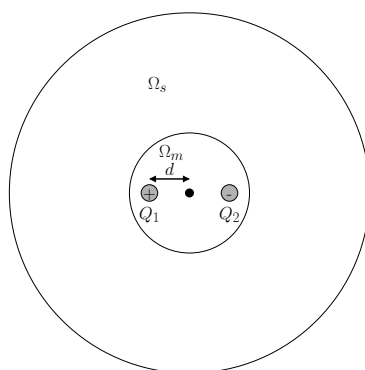


Figure 9: Domain for a simple dipole.

Dipole

In this section we illustrate the performance of our scheme on a simple dipole, as depicted in Figure 9. The linearized PBE for ions inside a spherical molecular region has been studied in [58]. For our experiment the domain consists of a spherical molecular region of radius 2 units, with two equal, but opposite unit charges, q^+ and q^- , inside. The charges are placed on opposite sides of the x-axis, each at distance d from the origin (see Figure 9). As d is increased, the charges move closer to the interface, the solution becomes less well-behaved, developing a sharp gradient at the interface. Uniform refinement does not efficiently resolve the solution in this scenario. However, adaptive refinement is able to refine locally around the simplices at the interface, and gives

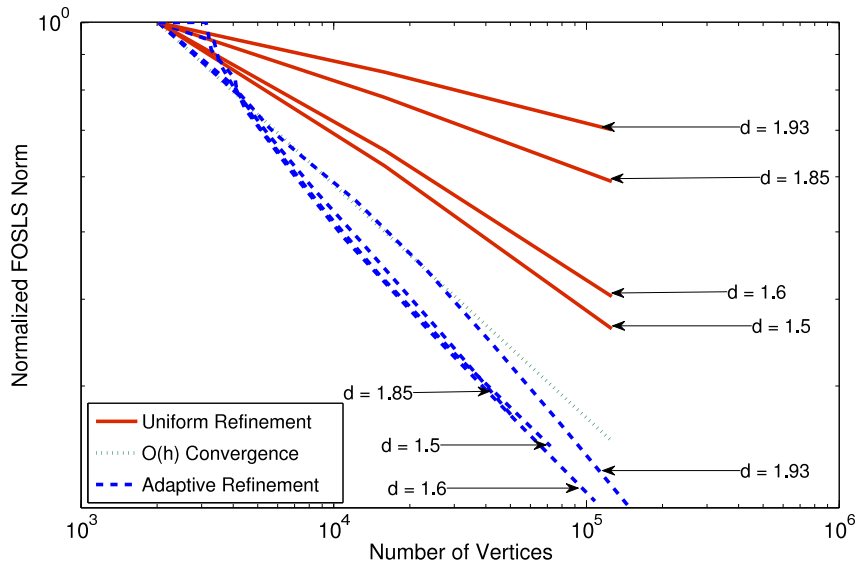


Figure 10: FOSLS functional convergence rates for a simple dipole

a significantly better convergence rate than uniform refinement as shown in Figure 10. In particular, the rate of convergence for adaptive refinement is nearly insensitive to changes in the parameter d .

1BOR

Finally, we compute the electrostatic solvation free energy of transcription factor PML (PDB code 1BOR), and compare our value with the results in [59], where they choose $\epsilon_m = 1$, $\epsilon_s = 80$. The electrostatic free energy of solvation is defined by [59]

$$\Delta G_{sol} = \frac{1}{2} \sum_{j=1}^{n_s} Q_j (\phi(x_j) - \phi_{homo}(x_j)), \quad (38)$$

where ϕ_{homo} is the solution of equation 2a in homogenous enironment, thats is $\epsilon_m = \epsilon_s = 1$. In terms of the regularized potential u , the solvation free energy can be computed as,

$$\Delta G_{sol} = \frac{1}{2} \frac{k_B T}{e_c} \sum_{j=1}^{n_s} Q_j u(x_j) \quad (39)$$

On a mesh with 131086 vertices, we compute the free energy of solvation equal to -792.577 kcal/mol, which compares well with the value of -853.7 kcal/mol computed from the MIBPB-III method in [59]. The free energy of solvation is sensitive to the geometry of the protein surface. We use GAMer to define this interface geometry, and hence our result does not exactly match up with [59], who use MSMS [60] to generate their protein surface.

5. Conclusion

The interface jump condition in (11) presents a challenge to design a single-domain FOSLS approach. We overcome this difficulty with a choice of a vector parameter \mathbf{q} that results in a consistent and well-posed first-order system. The approach is also useful for solving the non-linear equation using a Newton-FOSLS method [61], as each step of Newton's method will effectively involve solution of a linearized Poisson-Boltzmann equation. In this paper we show that the resulting FOSLS functional defines a norm equivalent to the norm on $H^1 \times H(\text{div})$, yet can be used in an existing finite element framework that uses more standard piecewise continuous elements in H^1 .

We offer numerical evidence in support of this approach and test the methodology on several problems. We observe that adaptive refinement based on the FOSLS functional scheme yields a faster convergence rate than uniform refinement, and that this effect is more pronounced for solutions that are more sharply varying.

References

- [1] N. A. Baker, D. Bashford, D. A. Case, Implicit solvent electrostatics in biomolecular simulation, in: B. Leimkuhler, C. Chipot, R. Elber, A. Laaksonen, A. Mark, T. Schlick, C. Schutte, R. Skeel (Eds.), *New Algorithms for Macromolecular Simulation*, Vol. 49 of Lecture Notes in Computational Science and Engineering, Springer-Verlag, 2006, pp. 263–295.
- [2] D. Bashford, D. A. Case, Generalized Born models of macromolecular solvation effects, *Annu. Rev. Phys. Chem.* 51 (1) (2000) 129–152.
- [3] L. Chen, M. J. Holst, J. Xu, The finite element approximation of the nonlinear Poisson-Boltzmann equation, *SIAM J. Numer. Anal.* 45 (6) (2007) 2298–2320.
- [4] F. Fogolari, P. Zuccato, G. Esposito, P. Viglino, Biomolecular electrostatics with the linearized Poisson-Boltzmann equation., *Biophys. J.* 76 (1) (1999) 1–16.
- [5] F. Fogolari, A. Brigo, H. Molinari, The Poisson-Boltzmann equation for biomolecular electrostatics: A tool for structural biology, *J. Mol. Recognit.* 15 (6) (2002) 377–392.
- [6] I. Klapper, R. Hagstrom, R. Fine, K. Sharp, B. Honig, Focusing of electric fields in the active site of Cu-Zn superoxide dismutase: Effects of ionic strength and amino-acid modification, *Proteins: Struct. Funct. Genet.* 1 (1) (1986) 47–59.
- [7] J. Warwicker, H. C. Watson, Calculation of the electric potential in the active site cleft due to alpha-helix dipoles, *J. Mol. Biol.* 157 (4) (1982) 671–679.
- [8] M. K. Gilson, K. A. Sharp, B. H. Honig, Calculating the electrostatic potential of molecules in solution: Method and error assessment, *J. Comput. Chem.* 9 (1987) 327–335.
- [9] M. E. Davis, J. A. McCammon, Solving the finite difference linearized Poisson-Boltzmann equation: A comparison of relaxation and conjugate gradient methods, *J. Comput. Chem.* 10 (1989) 386–391.
- [10] M. J. Holst, F. Saied, Numerical solution of the nonlinear Poisson-Boltzmann equation: Developing more robust and efficient methods, *J. Comput. Chem.* 16 (1995) 337–364.
- [11] N. A. Baker, D. Sept, S. Joseph, M. J. Holst, J. A. McCammon, Electrostatics of nanosystems: Application to microtubules and the ribosome, *Proc. Natl. Acad. Sci. USA* 98 (2001) 10037–10041.
- [12] B. A. Luty, M. E. Davis, J. A. McCammon, Solving the finite-difference non-linear Poisson-Boltzmann equation, *J. Comput. Chem.* 13 (9) (1992) 1114–1118.
- [13] D. Bashford, An object-oriented programming suite for electrostatic effects in biological molecules An experience report on the MEAD project, in: *Scientific Computing in Object-Oriented Parallel Environments*, Vol. 1343 of Lecture Notes in Computer Science, 1997, pp. 233–240.
- [14] W. Rocchia, E. Alexov, B. Honig, Extending the applicability of the nonlinear Poisson-Boltzmann equation: Multiple dielectric constants and multivalent ions, *J. Phys. Chem. B* 105 (28) (2001) 6507–6514.
- [15] Y. C. Zhou, G. W. Wei, On the fictitious-domain and interpolation formulations of the matched interface and boundary (MIB) method, *J. Comput. Phys.* 219 (1) (2006) 228–246.
- [16] W. H. Orttung, Direct solution of the Poisson equation for biomolecules of arbitrary shape, polarizability density, and charge distribution, *Ann. N.Y. Acad. Sci.* 303 (1977) 22–37.
- [17] C. M. Cortis, R. A. Friesner, Numerical solution of the Poisson-Boltzmann equation using tetrahedral finite-element meshes, *J. Comput. Chem.* 18 (1997) 1591–1608.
- [18] M. J. Holst, N. A. Baker, F. Wang, Adaptive multilevel finite element solution of the Poisson-Boltzmann equation I: Algorithms and examples, *J. Comput. Chem.* 21 (2000) 1319–1342.
- [19] N. A. Baker, M. J. Holst, F. Wang, Adaptive multilevel finite element solution of the Poisson-Boltzmann equation II: Refinement at solvent accessible surfaces in biomolecular systems, *J. Comput. Chem.* 21 (2000) 1343–1352.
- [20] A. I. Shestakov, J. L. Milovich, A. Noy, Solution of the nonlinear Poisson-Boltzmann equation using pseudo-transient continuation and the finite element method, *J. Colloid Interface Sci.* 247 (1) (2002) 62–79.
- [21] D. Xie, S. Zhou, A new minimization protocol for solving nonlinear Poisson-Boltzmann mortar finite element equation, *BIT Numerical Mathematics* 47 (4) (2007) 853–871.
- [22] C. Wenbin, S. Yifan, X. Qing, A mortar finite element approximation for the linear Poisson-Boltzmann equation, *Appl. Math. Comput.* 164 (1) (2005) 11–23.
- [23] S. Miertus, E. Scrocco, J. Tomasi, Electrostatic interaction of a solute with a continuum. A direct utilization of AB initio molecular potentials for the prevision of solvent effects, *Chem. Phys.* 55 (1) (1981) 117–129.
- [24] R. Zauhar, R. Morgan, A new method for computing the macromolecular electric potential, *J. Mol. Biol.* 186 (4) (1985) 815–820.
- [25] A. A. Rashin, Hydration phenomena, classical electrostatics, and the boundary element method, *J. Chem. Phys.* 94 (5) (1990) 1725–1733.
- [26] B. J. Yoon, A. M. Lenhoff, A boundary element method for molecular electrostatics with electrolyte effects, *J. Comput. Chem.* 11 (9) (1990) 1080–1086.
- [27] A. H. Juffer, E. F. Botta, B. A. van Keulen, A. van der Ploeg, H. J. Berendsen, The electric potential of a macromolecule in a solvent: A fundamental approach, *J. Comput. Phys.* 97 (1) (1991) 144–171.
- [28] Y. N. Vorobjev, J. A. Grant, H. A. Scheraga, A combined iterative and boundary-element approach for solution of the nonlinear Poisson-Boltzmann equation, *J. Amer. Chem. Soc.* 114 (9) (1992) 3189–3196.
- [29] H.-X. Zhou, Boundary element solution of macromolecular electrostatics: Interaction energy between two proteins, *Biophys. J.* 65 (1993) 955–963.
- [30] R. Bharadwaj, A. Windemuth, S. Sridharan, B. Honig, A. Nicholls, The fast multipole boundary element method for molecular electrostatics: An optimal approach for large systems, *J. Comput. Chem.* 16 (7) (1995) 898–913.
- [31] Y. N. Vorobjev, H. A. Scheraga, A fast adaptive multigrid boundary element method for macromolecular electrostatic computations in a solvent, *J. Comput. Chem.* 18 (4) (1997) 569–583.
- [32] J. Liang, S. Subramaniam, Computation of molecular electrostatics with boundary element methods, *Biophys. J.* 73 (4) (1997) 1830–1841.
- [33] A. H. Boschitsch, M. O. Fenley, H.-X. Zhou, Fast boundary element method for the linear Poisson-Boltzmann equation, *J. Phys. Chem. B* 106 (10) (2002) 2741–2754.
- [34] B. Lu, D. Zhang, J. A. McCammon, Computation of electrostatic forces between solvated molecules determined by the Poisson-Boltzmann equation using a boundary element method, *J. Chem. Phys.* 122 (21) (2005) 214102.
- [35] S. S. Kuo, M. D. Altman, J. P. Bardhan, B. Tidor, J. K. White, Fast methods for simulation of biomolecule electrostatics, in: *ICCAD '02: Proceedings of the 2002 IEEE/ACM international conference on Computer-aided design*, ACM Press, New York, NY, USA, 2002, pp. 466–473.

- [36] B. Lu, X. Cheng, J. Huang, J. A. McCammon, Order N algorithm for computation of electrostatic interactions in biomolecular systems, *Proc. Natl. Acad. Sci. USA* 103 (51) (2006) 19314–19319.
- [37] Z. Cai, R. Lazarov, T. A. Manteuffel, S. F. McCormick, First-order system least squares for second-order partial differential equations. I, *SIAM J. Numer. Anal.* 31 (6) (1994) 1785–1799.
- [38] Z. Cai, T. A. Manteuffel, S. F. McCormick, First-order system least squares for second-order partial differential equations. II, *SIAM J. Numer. Anal.* 34 (2) (1997) 425–454.
- [39] T. A. Manteuffel, S. F. McCormick, G. Starke, First-order system least-squares for second order elliptic problems with discontinuous coefficients, in: N. D. Melson, T. A. Manteuffel, S. F. McCormick, C. C. Douglas (Eds.), *Seventh Copper Mountain Conference on Multigrid Methods*, Vol. CP 3339, NASA, Hampton, VA, 1996, pp. 535–550.
- [40] M. Berndt, T. A. Manteuffel, S. F. McCormick, G. Starke, Analysis of first-order system least squares (FOSLS) for elliptic problems with discontinuous coefficients. I, *SIAM J. Numer. Anal.* 43 (1) (2005) 386–408.
- [41] M. Berndt, T. A. Manteuffel, S. F. McCormick, Analysis of first-order system least squares (FOSLS) for elliptic problems with discontinuous coefficients. II, *SIAM J. Numer. Anal.* 43 (1) (2005) 409–436.
- [42] M. Holst, Adaptive numerical treatment of elliptic systems on manifolds, *Adv. Comput. Math.* 15 (1–4) (2001) 139–191.
- [43] P. B. Bochev, M. D. Gunzburger, Finite element methods of least-squares type, *SIAM Rev.* 40 (4) (1998) 789–837.
- [44] F. Brezzi, M. Fortin, *Mixed and hybrid finite element methods*, Vol. 15 of Springer Series in Computational Mathematics, Springer-Verlag, New York, 1991.
- [45] Y. Song, Y. Zhang, T. Shen, C. L. Bajaj, J. A. McCammon, N. A. Baker, Finite element solution of the steady-state Smoluchowski equation for rate constant calculations, *Biophys. J.* 86 (4) (2001) 2017–2029.
- [46] Y. Cao, M. D. Gunzburger, Least-squares finite element approximations to solutions of interface problems, *SIAM J. Numer. Anal.* 35 (1) (1998) 393–405.
- [47] V. Girault, P.-A. Raviart, *Finite element methods for Navier-Stokes equations*, Vol. 5 of Springer Series in Computational Mathematics, Springer-Verlag, Berlin, 1986.
- [48] M. Berndt, T. A. Manteuffel, S. F. McCormick, Local error estimates and adaptive refinement for first-order system least squares (FOSLS), *Electron. Trans. Numer. Anal.* 6 (1997) 35–43.
- [49] E. C. Cyr, *Numerical methods for computing the free-energy of coarse-grained molecular systems*, Phd, University of Illinois at Urbana-Champaign (2008).
- [50] Z. Cai, C. Westphal, An adaptive mixed least-squares finite element method for viscoelastic fluids of Oldroyd type, *J. Non-Newtonian Fluid Mech.* 159 (1–3) (2009) 72–80.
- [51] Z. Yu, M. Holst, Y. Cheng, J. A. McCammon, Feature-preserving adaptive mesh generation for molecular shape modeling and simulation, *J. Mol. Graph. Model.* 26 (8) (2008) 1370 – 1380.
- [52] M. J. Holst, *Multilevel methods for the Poisson-Boltzmann equation*, Phd, University of Illinois at Urbana-Champaign (1994).
- [53] M. Born, Volumen und hydrationswärme der ionen, *Zeitschrift für Physik* 1 (1920) 45–48.
- [54] M. H. le Du, P. Marchot, P. E. Bougis, J. C. Fontecilla-Camps, 1.9-Å resolution structure of fasciculin 1, an anti-acetylcholinesterase toxin from green mamba snake venom, *J. Biol. Chem.* 267 (31) (1992) 22122–22130.
- [55] Z. Radić, P. D. Kirchhoff, D. M. Quinn, J. A. McCammon, P. Taylor, Electrostatic influence on the kinetics of ligand binding to acetylcholinesterase: Distinctions between active center ligands and fasciculin, *J. Biol. Chem.* 272 (37) (1997) 23265–23277.
- [56] N. A. Baker, V. Helms, J. A. McCammon, Dynamical properties of fasciculin-2, *Proteins: Struct. Funct. Genet.* 36 (4) (1999) 447–453.
- [57] W. Humphrey, A. Dalke, K. Schulten, VMD – Visual Molecular Dynamics, *J. Molec. Graphics* 14 (1996) 33–38.
- [58] J. G. Kirkwood, Theory of solutions of molecules containing widely separated charges with special application to zwitterions, *J. Chem. Phys.* 2 (7) (1934) 351–361.
- [59] W. Geng, S. Yu, G. Wei, Treatment of charge singularities in implicit solvent models, *J. Chem. Phys.* 127 (11) (2007) 114106.
- [60] M. F. Sanner, A. J. Olson, J.-C. Spehner, Fast and robust computation of molecular surfaces, in: *SCG '95: Proceedings of the eleventh annual symposium on Computational geometry*, ACM, 1995, pp. 406–407.
- [61] A. L. Codd, T. A. Manteuffel, S. F. McCormick, Multilevel first-order system least squares for nonlinear elliptic partial differential equations, *SIAM J. Numer. Anal.* 41 (6) (2003) 2197–2209.